Received: 16 March 2024 | Revised: 20 May 2024 | Accepted: 31 May 2024 | Published online: 6 June 2024

RESEARCH ARTICLE

Archives of Advanced Engineering Science
2025, Vol. 3(4) 252–264
DOI: 10.47852/bonviewAAES42022837

BON VIEW PUBLISHING

Promoting Sustainable Green Infrastructure: Experimental and Numerical Investigation of Concrete Reinforced with Recycled Steel Fibers

Izhar Ahmad[1,*] **and Mehdi Shokouhian**[1]

[1]*Department of Civil and Environmental Engineering, Morgan State University, USA*

Abstract: Accumulation of waste tires and their respective fast increase are posing a great threat to the environment. Recycled steel fiber (RSF) extracted from the waste tires can be used in reinforced concrete considering proper fiber content and aspect ratio. Current research study aims to investigate the influence of RSF content (0.5%, 1.5%, and 2.25%) on the mechanical properties such as compressive strength, split tensile, and flexural strength of recycled steel fiber-reinforced concrete (RSFRC). The study also focused on developing numerical models such as fracture-plastic constitutive models using ATENA to validate the experimental results. The study was further extended by developing a slab model as a bus pad to find the behavior of RSFRC bus pad in response to the service loads and soil stiffness. In Baltimore City, inadequate design of bus pads posed strength and serviceability problems and needed to be investigated. From the test results, it was found that RSFRC mixture containing 1.5% RSF exhibited optimized behavior. Test results showed that 28-day compressive, split tensile, and flexural strength increased by 10.7%, 39.3%, and 10.4%, respectively, for the RSFRC mixture containing 1.5% RSF as compared to the control mixture without RSF and other RSF containing mixtures. The numerical model was developed and validated using experimental data. Various models of bus pads were then analyzed, focusing on their maximum load-bearing capacity and flexural toughness. It was observed that the maximum load-bearing capacity and flexural toughness of the bus pads increased with the use of RSFRC. These findings offer valuable insights for the construction industry, facilitating the efficient utilization of RSFRC in concrete applications.

Keywords: fiber-reinforced concrete, finite element methods, recycled steel fibers

1. Introduction

The role of public transit, especially buses in Baltimore City, is crucial in promoting sustainable transportation within the United States and ensuring accessibility for individuals without personal vehicles. Pavement design in those areas where buses frequently start and stop needs a special design such as replacing asphaltic pavement with the concrete. Therefore, concrete pads are preferred over the asphaltic pavement so as to prevent failure problems that happens with the asphaltic pavement. Similarly, inadequate design of bus pads poses strength and serviceability problems in the past and often results with cracking as found in Baltimore City [1]. Different studies have been carried out addressing the cracking issues of concrete bus pads and tried to improve the concrete properties subjected to vehicular loading. Concrete being the most versatile construction material still has several deficiencies for instance brittleness and limited ductility, lower tensile strength, and post-cracking capability [2–5].

The use of discrete steel fibers to strengthen cement-based materials is a common practice in various applications, such as hydraulic structures, bridges, and linings of tunnel [6]. Similarly, concrete reinforced with steel fibers is utilized in both precast and on-site concrete elements, enabling the complete or partial replacement of traditional rebars. This approach decreases cost of labor and construction time associated with placing conventional rebars [7]. Researchers have been investigating the addition of industrial steel fibers (ISF) in cement-based materials for the past three decades to enhance the mechanical and durability performance of these structures. It has been reported that steel fiber reinforcement in concrete also helps minimize cracking caused by shrinkage and enhances the long-term durability of concrete structures [8–10]. The addition of ISF in concrete helps in restraining the crack opening, leading to a significant increase in energy absorption and load-bearing capacity after cracking [9]. The stress redistribution facilitated by fiber reinforcement enables the ultimate load to surpass the cracking load, which proved to be highly advantageous for concrete structures possessing a substantial level of support redundancy [11].

Recent studies indicated that recycled steel fibers (RSF) can serve as a sustainable substitute to commercial ISF in steel

*Corresponding author: Izhar Ahmad, Department of Civil and Environmental Engineering, Morgan State University, USA. Email: izhar.ahmad@morgan.edu

fiber-reinforced concrete (SFRC), while maintaining the essential mechanical properties, as long as the RSF possesses appropriate geometric features [12, 13]. Numerical studies based on experiments focusing on the bond behavior and tensile properties of RSF rooted in cementitious composites have demonstrated improved ductile behavior of RSFRC [14–16]. Several research groups have already successfully implemented RSF in concrete [12, 17–21]. It has been observed that RSF has the potential to be a highly promising alternative to ISF, although it is likely that higher RSF loadings would be required in concrete to achieve comparable effects in terms of mechanical properties [12]. Further comparisons have also demonstrated that RSF can match the shear performance of ISF [19]. However, the lack of guidelines and design protocols for RSF concrete significantly restricts its practical applications. Therefore, to bridge the gap between laboratory-scale tests and commercial implementation, further research aiming to develop a mathematical model is important.

Experimental and numerical investigations have been conducted to study the behavior of fiber-reinforced concrete (FRC) slabs used in rigid pavements. Belletti et al. [22] conducted laboratory tests on various FRC slabs having various aspect ratios and volumes of fibers. Slabs were supported by springs simulating a subgrade proposed by Winkler, and a finite element method was employed for numerical simulation of nonlinear behavior. The experimental and numerical results showed good agreement, providing valuable insights for design considerations [22]. ANSYS was used for the modeling of concrete pavements in which solid brick elements were used to represent the concrete slab, whereas spring elements were used to represent the soil [23]. The analysis considered various loads and employed elastic springs to represent the soil behavior. Soil stiffness was determined by the subgrade reaction modulus. The research compared the stress results obtained from the finite element method with conventional approaches such as Indian Road Congress and Westergaard's method, contributing to a better understanding of pavement behavior. In another study, ABAQUS was used for the simulation of bending test of SFRC specimens. 3-D models of three-point bending tests were created, and static loads were applied until reaching maximum values. Different percentages of steel fibers such as 0, 0.4, and 0.8% were included in the beam specimens of SFRC. The experimental and analytical results demonstrated that magnitudes of stress, strain, and deflection increased proportionally with the addition of steel fibers [24]. However, research on numerical analysis employing ATENA as finite element software utilizing RSF in rigid pavements is limited, and further investigation is needed to understand the behavior of RSFRC bus pads under vehicular loadings. It is also pertinent to mention that subgrade soil condition varies from state to state, therefore it is also necessary to determine the effect of existing subgrade soil behavior on the load carrying capacity of bus pads.

This research study explored a new material model to simulate RSFRC bus pads numerically. The impact of incorporating RSF into concrete was investigated in the laboratory to understand its effects on mechanical properties. The findings from these tests formed the basis for developing a material model used in subsequent numerical simulations. ATENA Studio v5 software [25], known for its strong capabilities in nonlinear analysis of FRC, was utilized to perform the numerical simulations of tested beams. In this software, inverse analysis was employed to match the stress-strain relationship observed in the experimental study. The main objective of this paper was to create a practical and relatively straightforward numerical tool for analyzing RSF-reinforced concrete. Importantly, this approach could potentially pave the way for new technological applications of RSFRC in construction. The study primarily focused on the following objectives:

1) To investigate the influence of RSF on the mechanical properties such as compressive strength, split tensile strength, and flexural strength of RSFRC.
2) To establish analytical equations which will predict the actual strength behavior of the RSFRC.
3) To develop numerical models for predicting the maximum load carrying capacity of RSFRC bus pads.
4) To find the influence of the subgrade soil on the load carrying capacity of the RSFRC bus pads.

2. Experimental Study

Experimental investigation was performed to evaluate the influence of RSF on the mechanical properties such as compression, split tensile, and flexural strength of RSFRC. For this purpose, various concrete mixtures were cast based upon RSF content such as 0%, 0.5%, 1.5%, and 2.25%, respectively. Experimental program is proceeded as the following subsections.

2.1. RSF extraction and sorting

RSF obtained were analyzed by separating the steel fibers from tire rubber, and thus various percentages of steel fibers were observed. The highest proportion of steel fibers that were not mixed with rubber was found within the 3%–6% range. Before employing RSF in concrete, rubber-free clean RSFs were obtained, as can be seen in Figure 1, respectively. After separation, sorting and characterization of RSF were performed. For the purpose of this investigation, steel fibers were manually sorted, and sizes of the fibers were determined such as length and diameter, as can be seen in Figure 2.

2.2. Geometric characterization

Geometric characterization of the RSFs was imperative as it influences the properties of RSFRC. The number of fibers incorporated to the concrete mix was measured as a percentage of the total weight of the concrete plus RSF, also known as weight fraction. Aspect ratio was determined by dividing fiber length (l) by its diameter (d). In the current study, a batch of RSF was grabbed randomly consisting of almost 500 RSFs, and the length and the diameter of each fiber were determined manually using a ruler and a vernier caliper, respectively. Measurement of the

Figure 1
Recycled steel fibers: (a) RSF with tire rubber and (b) RSF separated from tire rubber

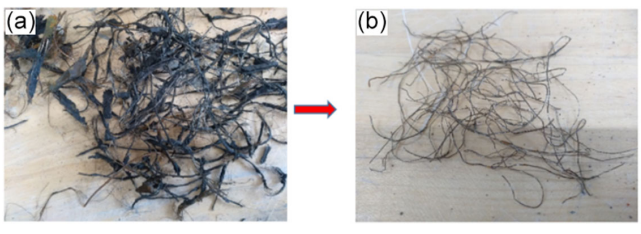

Figure 2
Length and diameter of RSF sample measured with vernier caliper

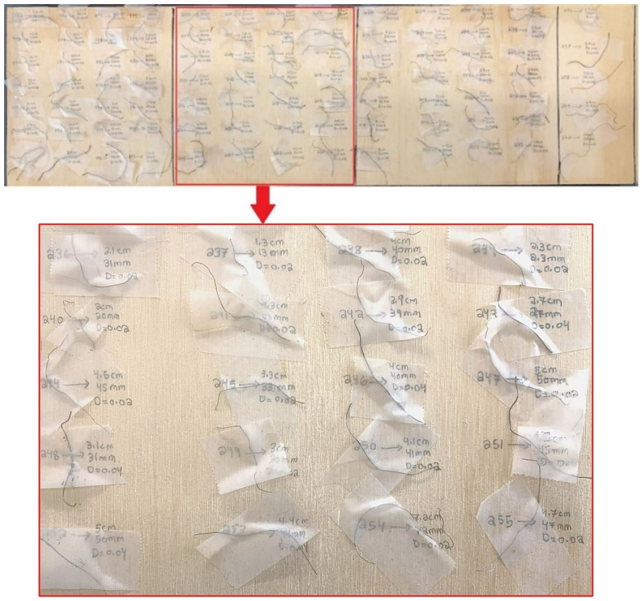

diameter using vernier caliper was performed with proper care so as to not underestimate cross-section of the macro fiber. Statistical data analysis of the RSF batch showed that most lengths were between 20 mm and 60 mm, varying between 3% and 12%. Similarly, 0.2 mm diameter and an aspect ratio of 125 occurred the most with a frequency of 67.4% and 15.4%, respectively.

2.3. Mix proportions

RSF was incorporated to concrete mix at three different percentages such as 0.5%, 1.5%, and 2.25%. Four groups of mixes were prepared and were differentiated based on percentage of RSF such as control mix (CM), RCM-0.5, RCM-1.5, and RCM-2.25 corresponding to CM having no RSF, RSFRC mix containing 0.5% RSF, RSFRC mix containing 1.5% RSF, and RSFRC mix containing 2.25% RSF, respectively. A total of 42 specimens were made, which consisted of 20 specimens for compression (101.6 × 203 mm cylinder), 12 specimens for split tensile strength test (101.6 × 203 mm cylinder), and 12 for flexural strength test (534 × 152 × 152 mm beam), as shown in Table 1. Type 1 ordinary Portland cement meeting ASTM C150 specifications was used in the current study [26]. Fine aggregate and coarse aggregate used were locally available in the market. Specific gravity of fine aggregate was 2.64, having water absorption of 0.7% and fineness modulus of 2.80, conforming to ASTM C33 [27]. Similarly, the coarse aggregates were well graded having maximum gravel size of 19mm with a specific gravity of 2.68, water absorption of 0.5%, and unit weight of 1602 kg/m^3. Mix proportioning for the concrete is shown in Table 2. Mixing of cement, sand, and coarse aggregate was done following ASTM C192 [28]. RSF was timely incorporated to the concrete mixer in order to avoid clumping of the fibers. A constant water-cement ratio of 0.47 was maintained in all the mixes. After mixing the concrete was cast into the cylinder and beam molds and kept at room temperature. The specimens were taken out of the molds after 24 h and placed in the curing tank for

Table 1
Scheme of experimental testing

Mixtures	Compressive test specimens	Flexural test specimens	Split tensile test specimens
CM	5	3	3
RCM-0.5	5	3	3
RCM-1.5	5	3	3
RCM-2.25	5	3	3

Table 2
Mix proportions

Mixtures	RSF %	Cement	Coarse aggregate	Fine aggregate	Water
		kg/m^3			
CM	0	410	1073	728	193
RCM-0.5	0.75	410	1073	728	193
RCM-1.5	1.5	410	1073	728	193
RCM-2.25	2.25	410	1073	728	193

the specified period of time. Experimental work was conducted in the Structure Laboratory at Morgan State University, as shown in Figure 3.

2.4. Testing methods

Slump test was carried out in order to know about workability of both control and RSFRC mixes. ASTM C143 [29] was followed by conducting the slump test. Slump cone was placed on the flat leveled surface and filled with concrete in three equal layers. A tamping rod was used to compact each layer 25 times. Excess concrete was removed by the rolling motion of the tamping rod. The slump was determined as the vertical difference between the top of the mold and the top surface of the concrete specimen.

Compression strength of the concrete is considered as the most significant property as it indicates the overall quality of the concrete and the hydrated cement gel. Compressive strength testing was conducted following ASTM C39/C39M [30]. Concrete was poured in three layers in the molds and was tamped with the tamping rod. Surface of the concrete in the cylinder and beam mold was finished smooth by removing the surplus concrete with a sharp edging tool. After finishing, the samples were placed and kept for curing, and then, physical testing was carried out at 7, 14, and 28 days. Universal testing machine (Instron-1000HDX-C3-G7B) at Structures Lab, Morgan State University was employed for compression, flexural, and split tensile testing, as shown in Figure 4. Compressive strength was directly calculated by the UTM which is the load resisted by the surface area of the cylinder. An average of the five specimens was taken as the compression strength result was representative of the average of the three specimens.

Split tensile strength test was conducted following ASTM C496 [31]. Preparation of specimens for split tensile testing was same as for compressive strength with the same size of cylinder as 101.6 × 203 mm. However, for testing bearing strips were used and the cylinders were placed in the horizontal position along their length, as shown in Figure 4(c). Splitting tensile strength was determined by using Equation (1). The splitting tensile strength result was representative of the average of the three specimens.

Figure 3
Experimental work: (a) concrete mixer, beam, and cylinder molds, (b) fresh concrete and (c) casted beam and cylinder specimens

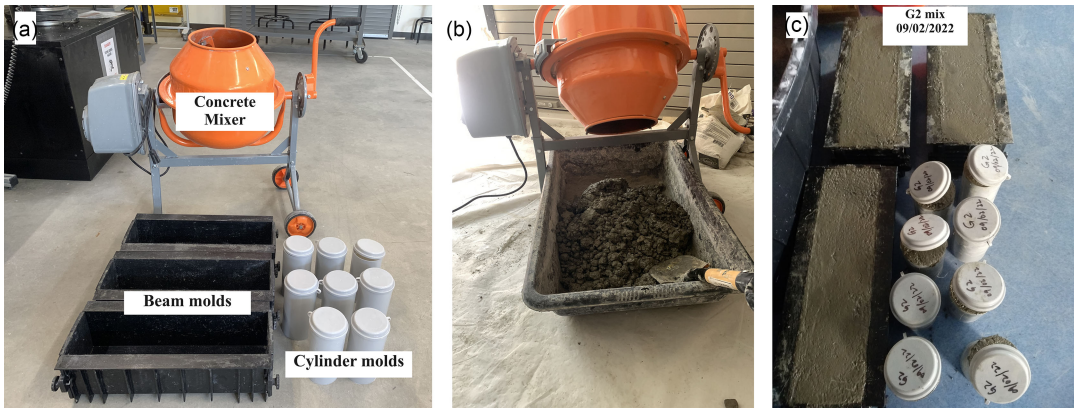

Figure 4
Mechanical properties testing: (a) cylinders and beam specimens, (b) compressive strength testing, (c) split tensile strength testing and (d) flexural strength testing

$$T = \frac{2P}{\pi ld} \quad (1)$$

Where:

T = Splitting tensile strength (MPa)
P = Maximum load (N)
l = Cylinder length (mm)
d = Cylinder diameter (mm)

Flexural strength test was conducted following ASTM C78 [32]. Third point loading method was used to determine the flexural strength of beam specimens having size of 534 × 152 × 152 mm. The beam specimens were loaded in a continuous manner without a shock. A load rate of 0.9 to 1.2 MPa/min was applied until rupture occurred. Calculation of the flexural strength was carried out using the formula in Equation (2). Furthermore, flexural toughness was also calculated from the load-deflection diagrams for various (slab) bus pad models. Flexural toughness indicates the energy

Figure 5
Geometry of beam model

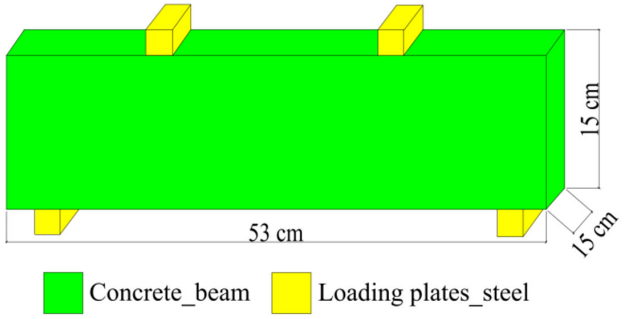

Figure 6
Geometry of bus pad model

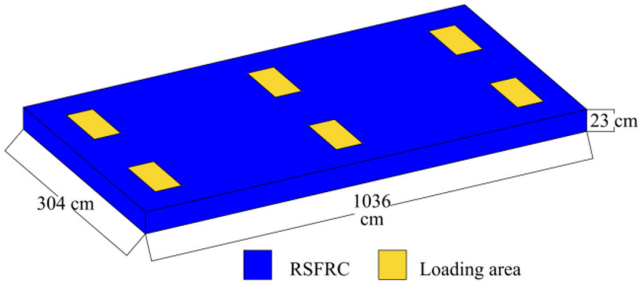

absorbed by the concrete and corresponds to the area under the load-displacement diagram [33]. It helps in assessing the post-cracking performance of RSFRC in flexure [34].

$$R = \frac{PL}{BD^2} \tag{2}$$

Where:

R = Flexure strength (MPa)
P = maximum load indicated by the UTM (N)
L = span length of beam (mm)
B = width of beam (mm)
D = depth of beam (mm)

3. Numerical Modeling

ATENA Studio was employed as the software for conducting nonlinear analysis developed by Cervenka Consulting. ATENA Studio accurately replicates the real performance of concrete structures, encompassing yielding of reinforcement, cracking of concrete, and its eventual crushing. Fracture-plastic constitutive model also named as CC3DNonLinCementitious2 was used as concrete model in the current study. The model is further comprised of two submodels for compression and tension called as plasticity model and fracture model, respectively [35]. Before the analysis of slab models, verification of beam models was conducted to confirm the actual simulation using GiD program for nonlinear analysis. Further, geometrical beam models were created where material properties and boundary conditions were defined. In this verification analysis, displacement and load were the parameters of interest. Initially, geometry of the beam model was developed having actual dimensions (53 cm × 15 cm × 15 cm) as were adopted during the experimental program, as illustrated in Figure 5. After developing geometry of the beam models, further geometry of the loading and supporting plates was designed such that steel plates were used as loading plates on top of the beam and as supporting plates at the bottom of the beam. After geometry creation, materials were defined for concrete and steel plates. CC3DNonLinCementitious2 was chosen as a material prototype with basic properties as obtained from the experiments and was given as input to the model. Similarly, the loading and supporting steel plates were chosen as Elastic 3D with CC3DElastIsotropic material prototype. The defined materials were then assigned to the geometrical models. Boundary conditions such as monitors, supports, and displacement were defined after the materials' definition. Since the purpose was to find the maximum load-bearing capacity of the beam, prescribed displacements were applied on the middle of the top loading plates. Here the beam was supported by the bottom steel plates in the vertical direction therefore the constraint condition was assigned to the bottom of each plate. Monitors play an important role in providing vital information about the condition of a structure. They are capable of tracking and observing various significant parameters throughout the analysis process. For example, it can be valuable to monitor the progression of deflections or strains at specific critical points during nonlinear analysis. In the current study, two monitors were assigned to the beam on the middle of the top plates for monitoring the loads and displacement of the beam, respectively. A structured meshing was performed for the beam model and then the model was run in GiD.

The slab model geometry was adopted as 304 cm wide, 1036 cm long, and 23 cm thick as shown in Figure 6. Concrete material was selected as CC3DNonLinCementitious2 based on the fracture-plastic constitutive model. Similarly, for RSFRC, the material model CC3DNonLinCementitious2User was adopted, which is commonly used for FRC in ATENA, combines both constitutive models for plastic and fracturing behavior. For loading surfaces, elastic 3D material was chosen having CC3DElastIsotropic material prototype. For steel bars, 1D reinforcement was chosen with a typical yielding strength of 500 MPa. Furthermore, rigid plates were used to simulate a loading condition at the places on the slab where the wheels of a bus would create maximum loading. Loading was assigned by prescribing the uniform vertical displacement of about 5 mm at the top surface of the steel plates. In this case, monitors were defined as a point condition on the middle of the top loading surfaces of the slab for monitoring the displacement and the maximum load in the *z*-direction, which helped in obtaining the load-displacement diagram. Similarly, the displacement condition was also assigned on the same points as monitors were applied. Side surfaces of the slab were applied as *x-y* constraint boundary condition according to the field observation. Since the top loading surfaces and the slab surface are two independent surfaces; therefore, a fixed contact between these two independent surfaces must be introduced so as to prevent sliding of the surfaces during analysis. The top loading surfaces were considered slave surfaces while the top surface of the slab was considered as a master surface condition. In finite element analysis, quality of the mesh element significantly influences the quality of analysis results, memory requirements, and the speed. Therefore, a structured meshing method with a hexahedron element type was adopted having a mesh size of 0.1.

In the context of flexible pavements, they are modeled as plates or beams supported by a flexible foundation. This study is focused on the analysis of a pavement with support from a Winkler spring foundation [36–39]. The Winkler foundation model represents the foundation as a series of evenly spaced and independent linear

Figure 7
Winkler soil-slab model

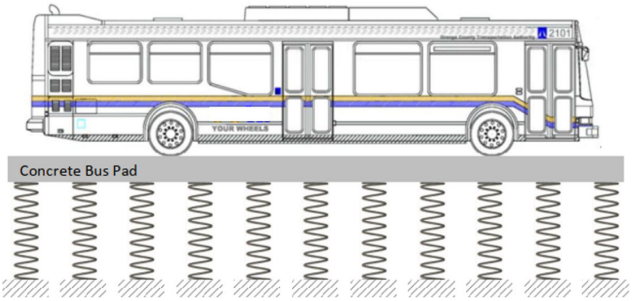

springs positioned beneath the beam/plate. According to this model, the nearby springs do not transmit load to each other, and each spring deforms solely in response to the vertical tension applied directly to it. Westergaard [40] utilized these types of pavement support systems in his own study. The subgrade reaction modulus of the supporting layer, which represents the stiffness of the springs in the current formulation (as shown in Figure 7), is theoretically equal to the spring constant. In the current study, the subgrade reaction modulus was adopted as 20,000 kN/m^2/m, based on the medium-dense sand condition of the site [1].

4. Results and Discussion

4.1. Workability

Slump cone method was used to determine the workability of the control and RSFRC mixes. It was found that workability of concrete was affected by the addition of RSF. The slump value recorded for the CM was 162 mm which decreased by 13.5%, 23.2%, and 28% for RCM-0.5, RCM-1.5, and RCM-2.25, respectively. It was concluded that the addition of RSF in concrete affects the workability of concrete. With the increase in the content of RSF from 0.5% to 2.25%, the workability of the concrete decreased as expressed from the results of the slump test. The same results were reported in previous researches such that using the same water-cement ratio the workability of RSFRC mixes reduced with the increasing content of RSF in concrete [17, 41–43]. The reason for this decrease in workability was due to the improved cohesive forces between the higher surface area of the elongated RSF and the matrix. Additionally, the presence of fibers can alter the granular fabric structure and create separation between particles. Moreover, the haphazard distribution of steel fibers in the mixtures hinders the flow of concrete [44]. It was stated in JGJT-2019 [45] that for pump-able concrete upto 30 m, the required slump needs to be in the range of 100 and 140 mm; thus in the current stud, workability of RCM-1.5 and RCM-2.25 met the required pumping criteria. It must be noted that the slump results do not reflect the quality of hardened concrete directly yet they provide information about the workability and pumping ability of fresh concrete and in the current study mixes with 1.5 and 2.25% RSF met the concrete pumping requirements.

4.2. Compressive strength

Compressive strength results for both CM and RSFRC mixes are shown in Figure 8. It has been noticed that with the increase in the percentage of RSF from 0 to 0.5%, 1.5%, and 2.25%, the compressive strength behavior improved at all ages such as 7 day, 14 day, and 28 day, respectively. At 7 day, an increase of 5.5%,

Figure 8
Compressive strength of concrete mixes with various RSF content

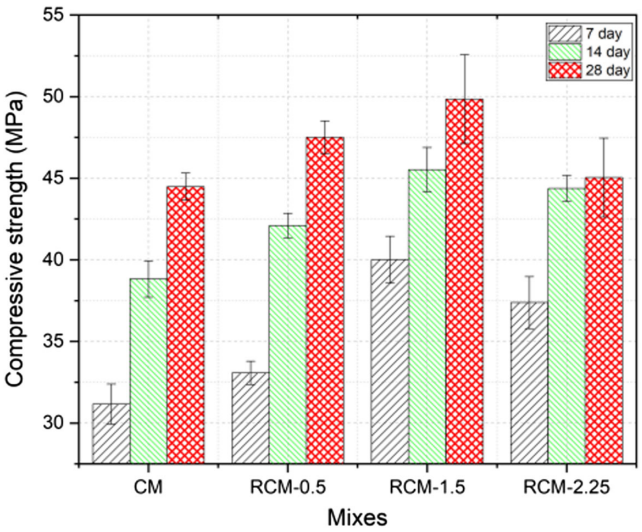

22%, and 16% in the compressive strength was noted for RCM-0.5, RCM-1.5, and RCM-2.25 mixtures, respectively, as compared to the CM. Similarly at 14 day, an increase of 7.6%, 15.5%, and 12.0% in the compressive strength was noted for RCM-0.5, RCM-1.5, and RCM-2.25 mixtures, respectively, as compared to the CM. Furthermore at 28 day, an increase of 6.3%, 10.7%, and 1.10% in the compressive strength was noted for RCM-0.5, RCM-1.5, and RCM-2.25 mixtures, respectively, as compared to the CM. However, at 28 day no substantial rise in the compression strength was noted for RCM-2.25 mix, and it was due to the increase in the number of fragile lines (an interface between the RSF and the cementitious paste) in unit area of a concrete cylinder. Similarly, according to Shah et al. [46], the high content of RSF in concrete increases the weak links between RSF and cement paste, thereby reducing the compressive strength of the concrete. However, Chen et al. [41] attributed decrease in the compression strength with high RSF content could be due to the differences in the fiber length distribution and concrete strength, and also for high fiber content, more mortar was used for enfolding the fibers which cause a decrease in compactness of the concrete mix. In support of the above results, Khaloo and Kim [3] reported that compression strength decreased because of the higher porosity when high volume of fibers is introduced into concrete.

From the results, it was revealed that within the same batch the compression strength increased with increasing the RSF content. It was indicated that RSF helped in increasing the compression strength capacity of RSFRC by bridging effect. The improvement in the compression strength behavior was due to the bond between the RSF and the concrete [47]. Other reasons for the improvement in the compression strength are due to the resistance offered by RSF and also due to confinement of concrete and these factors delay failure of the concrete section under compressive load.

It has also been reported by various other researchers that compression strength behavior of concrete improved with the incorporation of RSF as well as helped in increasing the ductile behavior of concrete [46, 47]. It was noticed that the failure pattern of the controlled concrete specimens having no RSF was quite different as compared to those containing RSF. The failure pattern of controlled concrete specimen was brittle and crumbled at a

Figure 9
Failure pattern of control and RSF specimens in compression

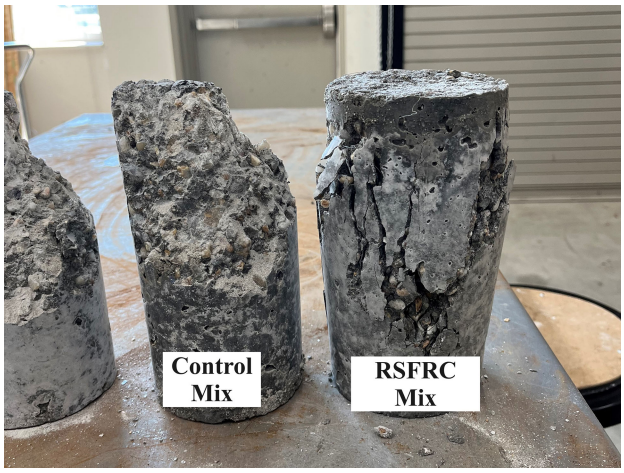

Figure 10
Splitting tensile and flexural strength of concrete mixes containing various percentages of RSF

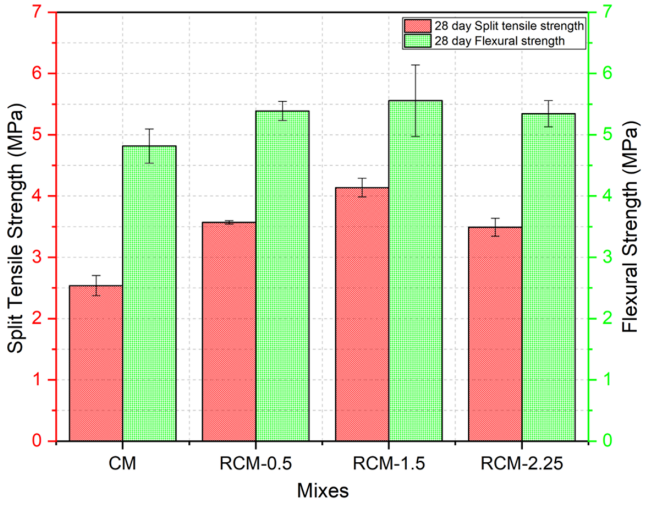

failure load. However, specimen containing RSF did not crumble at a failure load and showed a ductile failure, as illustrated in Figure 9. It was noticed that RSF specimens went through a slow deformation for long duration under a significant fraction of the peak load, and thus, residual strength of the concrete has also been increased as compared to CM. Results of the present research study were found in line with the past research by Hu et al. [48].

4.3. Split tensile strength

Evaluation of tensile capacity is a crucial parameter to measure the mechanical performance of plain concrete. Results of split tensile strength test for CM and RSFRC mixes are shown in Figure 10. It was noticed that with the increase in the dosage of RSF, splitting tensile strength of RSFRC specimens increased at 28 day. The split tensile strength increased from 2.5 to 3.02, 4.13, and 3.43 MPa for RCM-0.5, RCM-1.5, and RCM-2.25, respectively. Splitting tensile strength was increased from 0% to 16.8%, 39.3%, and 26.8% for RCM-0.5, RCM-1.5, and RCM-2.25, respectively. Enhancement in splitting tensile strength of the RSF-reinforced concrete was because of the resistance offered by the RSF to the propagation and widening of the cracks due to peak load. Furthermore, the results of the present research study were found in close agreement with past researches by Gul et al. [49].

4.4. Flexural strength

This test was conducted at 28 day for both CM and RSFRC specimens, and the results are depicted in Figure 10. From the results, it was noticed that the flexural strength behavior increased with the addition of RSF up to 1.5%. The flexural strength test increased from 4.98 to 5.39, 5.55, and 5.37 MPa for RCM-0.5, RCM-1.5, and RCM-2.25 mix, respectively. Similarly, flexural strength was increased from 0% to 7.6%, 10.4%, and 7.4% for RCM-0.5, RCM-1.5, and RCM-2.25 mixes, respectively. It was noted that in RSFRC specimens, the first crack appeared in the highest bending moment location at a load of 17 kN, 25 kN, and 18.8 kN for RCM-0.5, RCM-1.5, and RCM-2.25 mix, respectively, whereas in the case of CM the first crack appeared at an average load of 15.6 kN. It indicated that incorporation of RSF enhanced the elastic behavior of RSFRC specimens by 8.8%, 58.5%, and 20.4% for RCM-0.5, RCM-1.5, and RCM-2.25 mix, respectively. After the first appearance of the flexural crack, RSFRC specimens sustained 18.6% extra load as compared to the control specimens having no RSF. From Figure 11(b), it is shown that the presence of RSF helped the concrete to hold larger cracks before failure occurred, and it was due to the bridging action of RSF by keeping the fractured concrete sections and hence avoiding the brittle failure pattern as compared to the concrete with no RSF (Figure 11(a)). Similarly, presence of RSF improved the ultimate flexural load capacity by 2.4, 3.5, and 2.9 times as shown by the control specimens having no RSF. Thus, it is stated that incorporation of RSF in concrete helped in improving the pre-cracking and post-cracking stiffness leading to prevention of cracks widening at post-yield status, also reported in other studies by Gul et al. [49]. In summary, the influence of RSF content on the mechanical properties of concrete such as compression, split tensile, and flexural strength showed improvement in comparison to concrete having no RSF. However, this enhancement in mechanical properties was limited to the addition of RSF up to 1.5%, and upon exceeding, improvement in mechanical properties was decreased.

4.5. Prediction of strength behavior

The data analysis was conducted using OriginLab software. The fitting analysis was conducted by utilizing a nonlinear surface fit function, with input parameters including compressive strength, reinforcement index, and normalized peak point, for all scenarios investigated in the parametric study. Under the nonlinear surface, different functions including Power 2D, Exponential 2D, Polynomial 2D, Parabola 2D, Plane, Rational Tyle, and Rational 2D were tested. By putting the new equation obtained from each function result into an excel sheet, we were able to calculate percentage error for each function. As a result, of all the functions, polynomial 2D was found a reasonable fit for the current study; in other words, it means that Equations (3) and (4) obtained from fitting of the curves showed a least percentage difference between the strength results obtained from the experimental testing and analytical analysis as shown in Figure 12.

$$f_{crsf} = fc' + 5.3RI - 1.29RI^2 \ \text{(MPa)} \quad (3)$$

Figure 11
Flexural failure pattern of beam specimen: (a) control mix and (b) RCM-1.5

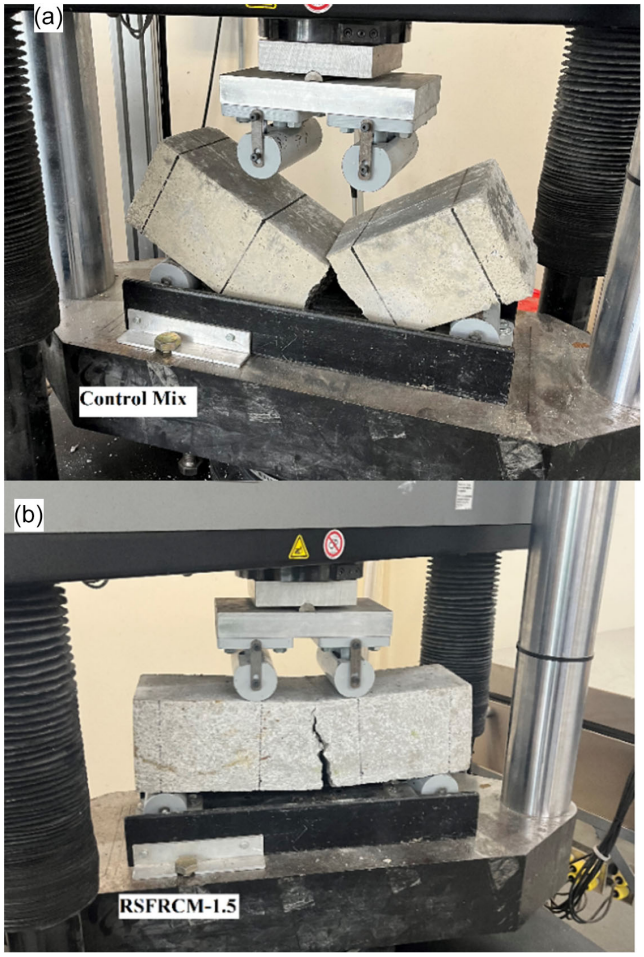

Figure 12
Experimental and analytical strength of various mixes: (a) compressive strength and (b) tensile strength

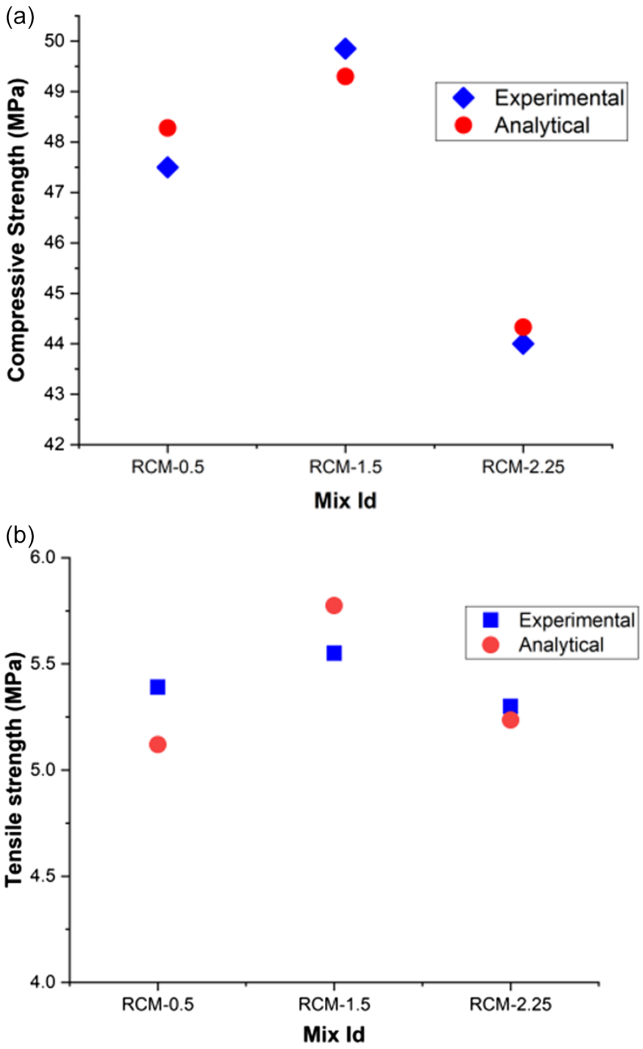

$$f_{trsf} = 0.63\sqrt{fc'} + 1.21RI - 0.232RI^2 \quad \text{(MPa)} \qquad (4)$$

Where:

f_{crsf} = compressive strength of RSFRC
$ftrsf$ = tensile strength of RSFRC
fc' = compression strength of concrete at 28 day
RI = reinforcement index

In previous studies by Shokouhian and Tsegaye [50], the equations developed for prediction of strength behavior were found to be based on the linear behavior of RSFRC; however in the current study, ascending and nonlinear trend was found in the experimental results of the compression, split tensile, and flexural strength, respectively. The compressive strength predicted through Equation (3) varied from the experimental results by 1.64, 1.10, and 0.75%, for RCM-0.5, RCM-1.5, and RCM-2.25, respectively. Similarly, tensile strength predicted through Equation (4) varied from the experimental results by 5.15, 3.97, and 1.22%, for RCM-0.5, RCM-1.5, and RCM-2.25, respectively.

4.6. Validation of numerical model

Geometrical model developed in ATENA-GiD was analyzed which resulted in the same failure pattern as exhibited during the experimental program. For specimens reinforced with RSF aided in bridging the cracks, indicating cracks were slowed and to a degree delayed their propagation. In all tests no rebars and stirrups were included as in the geometrical models, however, the results still exhibited an increase in the load the beam could bear. The final step of the verification process compared the load-displacement diagram of the experimental work and the numerical model from the ATENA analysis. In the experiment, crack occurred at the tension face in the middle third of the beam (Figure 11(b)); similarly, ATENA model showed tensile stress concentration and the corresponding crack width right at the tension face within the middle third of the beam as shown in Figure 13. However, during experimental testing of the RSFRC beam specimens exhibited failure not exactly in the middle third portion but near to the middle third portion of the beam on the tension face. The reason was due to the random distribution of the RSF within the beam which tend to fail the beam at the weakest zone, that is where the concentration of steel fibers was lower.

Similar to the control specimen, models for RSF specimens were developed with the input values obtained from the experiments. RSF inclusion in concrete increased the load

Figure 13
Failure pattern of the beam model after analysis

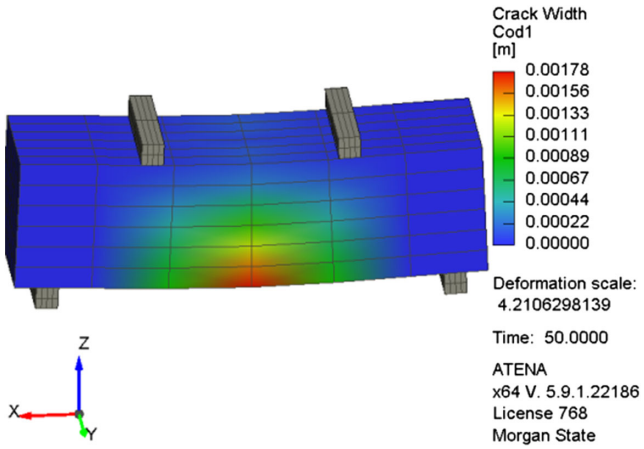

carrying capacity of the RSFRC beam. However, further addition of RSF beyond 1.5%, the increase in load carrying capacity was not much significant. The numerical models were analyzed and hence a little variation was noticed between the numerical and the experimental load-displacement curves at all percentage of RSF addition level as depicted in Figure 14. The difference recorded between the peak loads obtained from the numerical analysis and the experiment was 13%, 8%, 2%, and 0% for CM, RCM-0.5, RCM-1.5, and RCM-2.25, respectively. The simulation process assumes ideal conditions for materials and specimens, ensuring uniformity, isotropy, and consistent contact. However, in practical experiments materials exhibit some degree of anisotropy, and defects in casting and maintenance operations might lead to deviation in comparison results. Also, the beam size used in the flexural tests (specifically the ratio of width to depth, b/d) could have influenced the test outcomes. The adopted b/d ratio of 1 (width = 15 cm, height = 15 cm) might have contributed to size effects that affected the observed flexural strength values.

4.7. Analysis of slab model

Four different slab models were developed and analyzed. Properties such as compression and tensile strength for the concrete slab model were obtained from the experiments performed in the laboratory. However, for the RSFRC slab model with and without rebars, the strength results were obtained by thereby incorporating a reinforcement index having a fiber content of 1.5%. The following four slab models were analyzed in this study and their load-displacement (L-D) diagrams are shown in Figure 15.

1) Plain cement concrete (PCC) slab
2) RSFRC slab
3) PCC slab with reinforcement bars (PCC + Rebars or RCC)
4) RSFRC slab with reinforcement bars (RSFRC + Rebars)

Figure 15 depicts that the load-bearing capacity of the bus pad made of only concrete was increased by different percentages for each type of reinforcement. Specifically, RSFRC slab resulted in a 17% increase, PCC slab with rebars led to a 32% increase, and RSFRC slab with rebars resulted in a significant 154% increase when compared to the load-bearing capacity of a PCC slab. It was observed that reinforcement of concrete with RSF increased the

Figure 14
Load-Displacement diagram of ATENA model vs experimental data: (a) CM, (b) RCM-0.5, (c) RCM-1.5, and (d) RCM-2.25

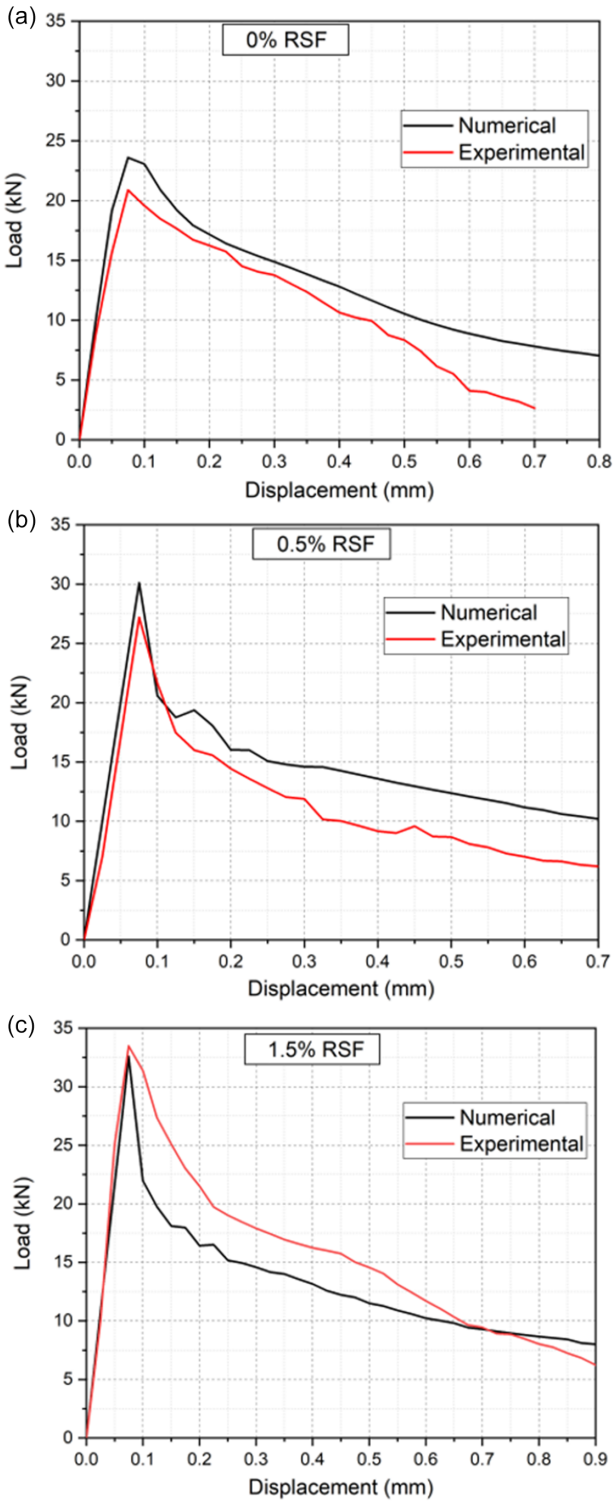

load-bearing capacity of the concrete slab however concrete reinforced with rebars has even greater load-bearing capacity in comparison to RSFRC slab. Therefore, for practical purposes, adding RSF to concrete with rebars will ultimately result in an improved load-bearing capacity. The presence of uniformly

Figure 14
(continued)

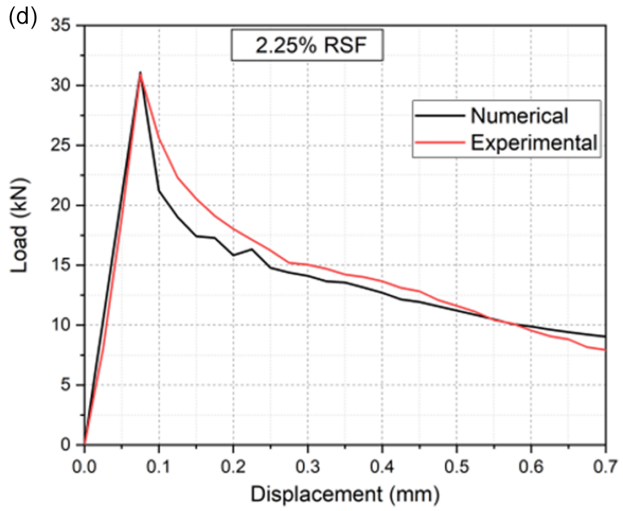

Figure 15
Load-Displacement diagram for different slab models

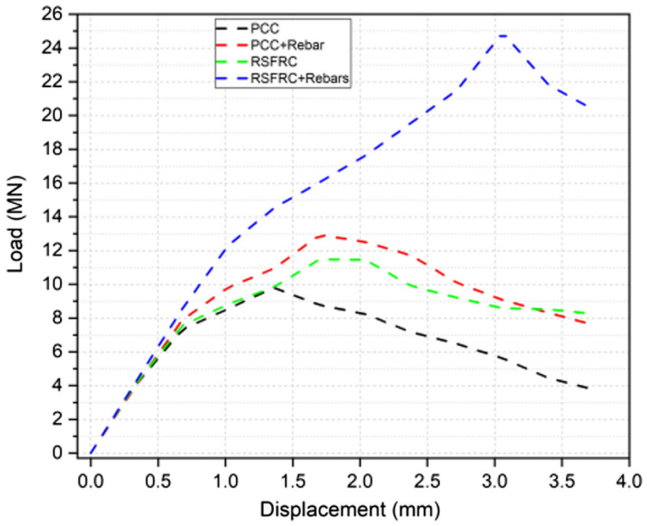

distributed RSF not only helped in the post-peak load-bearing capacity but also improved the ductile behavior of the section. This implies that the section will exhibit better resistance to cracking and enhanced flexibility. RSF are useful at both the serviceability and ultimate limit states by preventing cracking due to loads and raising the ultimate load capacity, respectively. Therefore, addition of RSF enhanced the flexural-tensile strength and post-cracking behavior of concrete. To conclude, RSF reinforcement significantly improved section behavior in terms of strength and ductility.

4.8. Flexural toughness

Flexural toughness for the various slab models was calculated from the load-displacement curves from the numerical analysis. The values of flexural toughness for slabs such as PCC, RSFRC, PCC + Rebars, and RSFRC + Rebars are provided in Table 3. It was

Table 3
Flexural toughness of bus pad models

Slab type	Peak load (MN)	Flexural toughness (MJ)
PCC	9.79	26.77
RSFRC	11.48	28.65
PCC + Rebars	12.9	32.26
RSFRC + Rebars	24.91	51.01

Figure 16
Effect of soil stiffness on load capacity of slab

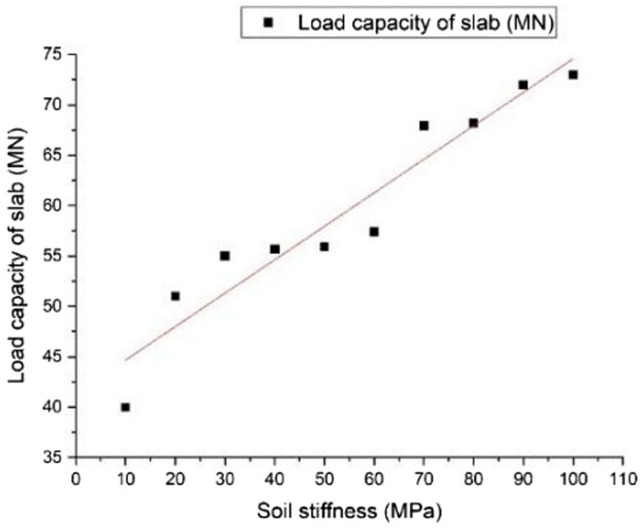

observed that the flexural toughness has increased by about 7% due to the inclusion of RSF and about 20% due to inclusion of rebars to PCC. Whereas due to inclusion of both (RSF and rebars), PCC has shown an increase of about 90% in flexural toughness. The results show that the incorporation of RSF alone or in combination with rebars into the slab enables it to bear loads even after appearance of the initial cracks. This transformation indicates a shift from brittle to ductile behavior [34, 51]. Thus incorporation of both RSF and rebars in concrete is highly beneficial for bus pads, as the flexural toughness and peak load will be increased since the bus pads experience heavy loads and need to withstand repeated loading cycles.

4.9. Soil stiffness

Load carrying capacity of the slab can be affected by the soil characteristics and specifically the soil stiffness. Load can be uniformly distributed when the soil is stiffer however when the soil is more flexible then the load can be distributed more locally rather than uniformly. From the numerical analysis of the slab, various soil types having different stiffness were used to evaluate the effect of soil stiffness on the load carrying capacity of the slab. Since the soil stiffness was considered as the main variable while the other input parameters such as modulus of elasticity, poison's ratio, tensile strength, and compressive strength were remained as constant as equal to 0.21, 29600 MPa, 5.55 MPa and 49.85MPa, respectively. After analysis, it was found that when the soil stiffness increased from 10 MPa to 100 MPa, and the load carrying capacity of the slab (RSFRC bus pad) increased by 43%, as shown in Figure 16. In other words, by ensuring proper compaction of the soil and higher stiffness of the soil and of the

bus pads will provide better resistance to the service loads from the buses. From Figure 16, it can be seen that, based on the current soil condition of the Baltimore City, if the soil stiffness is increased five times then the load carrying capacity of the bus pad can be increased by 43%, respectively.

5. Conclusion

Based on the experimental and numerical results, the findings of this research study are listed as follows.

1) Mechanical properties such as compressive strength, split tensile strength, and flexural strength of concrete improved with the incorporation of RSF. Maximum strength behavior was exhibited by RSFRC mix having 1.5% RSF. Compressive strength increased with the increase in the percentage of RSF. 28 day compressive strength increased by 6.3%, 10.7%, and 1.10% for RCM-0.5, RCM-1.5, and RCM-2.25, respectively. Further increase of RSF beyond 1.5% caused no significant improvement in the compressive strength. Improvement in the compressive strength was due to the resistance offered by the RSF under compressive load and also due to confinement of the concrete.
   28 day split tensile strength increased by 16.8%, 39.3%, and 26.8% for RCM-0.5, RCM-1.5, and RCM-2.25, respectively. Enhancement in split tensile strength of the RSFRC was due to the resistance offered by the RSF to the propagation and widening of the cracks due to peak load. Similarly, 28-day flexural strength increased by 7.6%, 10.4%, and 7.4% for RCM-0.5, RCM-1.5, and RCM-2.25, respectively. Presence of RSF helped the concrete to hold larger cracks before failure occurred and it was due to the bridging action of RSF by keeping the fractured concrete sections and hence avoiding the brittle failure pattern. Similarly, the presence of RSF enhanced the ultimate strength by preventing cracks from widening at post-yield status.
2) Predicted compressive and tensile strength values for RSFRC lied within 6% difference in the current study, indicating the practicability of the equations. The percentage difference between the experimental results and analytical results in case of compressive strength was 1.64, 1.10, and 0.75% for RCM-0.5, RCM-1.5, and RCM-2.25, respectively. Similarly, percentage difference in case of tensile strength was 5.15, 3.97, and 1.22% for RCM-0.5, RCM-1.5, and RCM-2.25, respectively.
3) A finite element analysis results were found close to the experimental results. The numerical analysis of beam using third point loading method yielded peak loads that differed from the experimental results by 8%, 2%, and 0% for RCM-0.5, RCM-1.5, and RCM-2.25, respectively. Based on the beam verification analysis, numerical analysis of different bus pads was performed. The peak loads obtained from the numerical analysis for PCC, RSFRC, PCC + Rebars, and RSFRC + Rebars were 9.8, 11.5, 12.9, and 24.9 MN, respectively. Hence, load carrying capacity of the bus pad increased by 17, 32, and 154% for RSFRC, PCC + Rebars, and RSFRC + Rebars, respectively, compared to the PCC slab without any reinforcement. Similarly, the inclusion of recycled fibers resulted in a 7% increase in flexural toughness, while the addition of rebars to PCC enhanced it by approximately 20%. Remarkably, incorporating both recycled fibers and rebars into PCC led to a substantial 90% increase in flexural toughness.
4) The load carrying capacity of the slab increased with the increase in the stiffness of the soil. Thus, soil having higher compaction and stiffness will better support the bus pads and will provide better resistance to the applied loads of the buses. From the numerical analysis, it was concluded that if the current soil stiffness of the Baltimore City bus stops is increased 5 times the load carrying capacity of the bus pads can be increased by 43%.

Furthermore, in order to confirm long-term durability of RSFRC bus pads, full-scale experimental investigation of RSFRC bus pads is required. Similarly, life cycle assessment analysis and environmental impact of RSFRC bus pads also need to be evaluated.

Acknowledgements

This research work was funded by a grant from the U.S. Department of Transportation's University Transportation Centers Program through the Center for Integrated Asset Management for Multimodal Transportation Infrastructure Systems.

Conflicts of Interest

The authors declare that they have no conflicts of interest to this work.

Data Availability Statement

Data are available from the corresponding author upon reasonable request.

Author Contribution Statement

Izhar Ahmad: Methodology, Software, Validation, Formal analysis, Investigation, Writing – original draft, Writing – review & editing, Visualization. **Mehdi Shokouhian:** Conceptualization, Methodology, Software, Resources, Writing – original draft, Writing – review & editing, Supervision, Project administration.

References

[1] Aslan, K., & Shokouhian, M. (2019). *Sustainable design of concrete bus pads to improve mobility in Baltimore City (Report No. UMEC-015)*. Urban Mobility & Equity Center. https://rosap.ntl.bts.gov/view/dot/40020

[2] Ahmad, I., Khan, K. A., Ahmad, T., Alam, M., & Bashir, M. T. (2022). Influence of accelerated curing on the compressive strength of polymer-modified concrete. *Frontiers of Structural and Civil Engineering*, *16*(5), 589–599.

[3] Khaloo, A. R., & Kim, N. (1997). Influence of concrete and fiber characteristics on behavior of steel fiber reinforced concrete under direct shear. *ACI Materials Journal*, *94*(6), 592–601.

[4] Khan, K. A., Ahmad, I., & Alam, M. (2019). Effect of ethylene vinyl acetate (EVA) on the setting time of cement at different temperatures as well as on the mechanical strength of concrete. *Arabian Journal for Science and Engineering*, *44*(5), 4075–4084. https://doi.org/10.1007/s13369-018-3249-4

[5] Khan, K. A., Nasir, H., Alam, M., Khan, S. W., & Ahmad, I. (2020). Performance of subgrade soil blended with cement and ethylene vinyl acetate. *Advances in Civil Engineering*, *2020*(1), 9831615. https://doi.org/10.1155/2020/9831615

[6] Frazão, C., Barros, J., Bogas, J. A., García-Cortés, V., & Valente, T. (2022). Technical and environmental

potentialities of recycled steel fiber reinforced concrete for structural applications. *Journal of Building Engineering*, *45*, 103579. https://doi.org/10.1016/j.jobe.2021.103579

[7] Domingo, M., Ramos, G., & Aparicio, Á. C. (2023). Use of fiber reinforced concrete in bridges – Metrorrey Line 2 case study. *Engineering Structures*, *276*, 115373. https://doi.org/10.1016/j.engstruct.2022.115373

[8] Bentur, A., & Mindess, S. (2006). *Fibre reinforced cementitious composites*. USA: CRC Press. https://doi.org/10.1201/9781482267747

[9] Cunha, V. M. C. F. (2010). *Steel fibre reinforced self-compacting concrete (from micromechanics to composite behavior)*. Doctoral Dissertation, University of Minho.

[10] Frazão, C., Camões, A., Barros, J., & Gonçalves, D. (2015). Durability of steel fiber reinforced self-compacting concrete. *Construction and Building Materials*, *80*, 155–166. https://doi.org/10.1016/j.conbuildmat.2015.01.061

[11] Salehian, H., Barros, J. A. O., & Taheri, M. (2014). Evaluation of the influence of post-cracking response of steel fibre reinforced concrete (SFRC) on load carrying capacity of SFRC panels. *Construction and Building Materials*, *73*, 289–304. https://doi.org/10.1016/j.conbuildmat.2014.09.043

[12] Caggiano, A., Folino, P., Lima, C., Martinelli, E., & Pepe, M. (2017). On the mechanical response of hybrid fiber reinforced concrete with recycled and industrial steel fibers. *Construction and Building Materials*, *147*, 286–295. https://doi.org/10.1016/j.conbuildmat.2017.04.160

[13] Tlemat, H., Pilakoutas, K., & Neocleous, K. (2006). Stress-strain characteristic of SFRC using recycled fibres. *Materials and Structures*, *39*(3), 365–377. https://doi.org/10.1007/s11527-005-9009-4

[14] Caggiano, A., Xargay, H., Folino, P., & Martinelli, E. (2015). Experimental and numerical characterization of the bond behavior of steel fibers recovered from waste tires embedded in cementitious matrices. *Cement and Concrete Composites*, *62*, 146–155. https://doi.org/10.1016/j.cemconcomp.2015.04.015

[15] Pająk, M., Krystek, M., Zakrzewski, M., & Domski, J. (2021). Laboratory investigation and numerical modelling of concrete reinforced with recycled steel fibers. *Materials*, *14*(8), 1828. https://doi.org/10.3390/ma14081828

[16] Pawelska-Mazur, M., & Kaszynska, M. (2021). Mechanical performance and environmental assessment of sustainable concrete reinforced with recycled end-of-life tyre fibres. *Materials*, *14*(2), 256. https://doi.org/10.3390/ma14020256

[17] Aiello, M. A., Leuzzi, F., Centonze, G., & Maffezzoli, A. (2009). Use of steel fibres recovered from waste tyres as reinforcement in concrete: Pull-out behaviour, compressive and flexural strength. *Waste Management*, *29*(6), 1960–1970. https://doi.org/10.1016/j.wasman.2008.12.002

[18] Groli, G., Pérez Caldentey, A., & Soto, A. G. (2014). Cracking performance of SCC reinforced with recycled fibres – An experimental study. *Structural Concrete*, *15*(2), 136–153.

[19] Leone, M., Centonze, G., Colonna, D., Micelli, F., & Aiello, M. A. (2018). Fiber-reinforced concrete with low content of recycled steel fiber: Shear behaviour. *Construction and Building Materials*, *161*, 141–155. https://doi.org/10.1016/j.conbuildmat.2017.11.101

[20] Pająk, M. (2019). Concrete reinforced with various amounts of steel fibers reclaimed from end-of-life tires. In *MATEC Web of Conferences, 262*, 06008. https://doi.org/10.1051/matecconf/201926206008

[21] Pająk, M. (2018). Application of fibers from end-of-life tires as a self-compacting concrete reinforcement–An experimental study. *Architecture, Civil Engineering, Environment*, *11*(1), 105–113. https://doi.org/10.21307/ACEE-2018-011

[22] Belletti, B., Cerioni, R., Meda, A., & Plizzari, G. A. (2004). Experimental and numerical analyses of FRC slabs on grade. In *Proceedings of FRAMCOS5 Conference*, 973–980.

[23] Khan, M. I., Khan, A. A., & Yadav, S. (2021). Mechanistic analysis of rigid pavement for wheel load stresses by finite element method considering different sub-grade with different percentage of metal fibre. *Indian Journal of Transport Engineering*, *1*(2), 1–9.

[24] Zimmer, J., Klein, D., & Stommel, M. (2015). Experimental and numerical analysis of liquid-forming. *Key Engineering Materials*, *651–653*, 842–847. https://doi.org/10.4028/www.scientific.net/KEM.651-653.842

[25] Cervenka, V., Jendele, L., & Cervenka, J. (2011). *ATENA program documentation. Theory and user manual*. Czech Republic: Cervenka Consulting.

[26] ASTM International. (2007). *Standard specification for Portland cement (ASTM C150)*. USA: ASTM International.

[27] ASTM International. (2016). *Standard specification for concrete aggregates (ASTM C33)*. USA: ASTM International.

[28] ASTM International. (2016). *Standard practice for making and curing concrete test specimens in the laboratory (ASTM C192)*. USA: ASTM International.

[29] ASTM International. (2012). *Standard test method for slump of hydraulic-cement concrete (ASTM C143/C143M-12)*. USA: ASTM International.

[30] ASTM International. (2017). *Standard test method for compressive strength of cylindrical concrete specimens (ASTM C39)*. USA: ASTM International.

[31] ASTM International. (2004). *Standard test method for splitting tensile strength of cylindrical concrete specimens (ASTM C496)*. USA: ASTM International.

[32] ASTM International. (2015). *Standard test method for flexural strength of concrete (using simple beam with third-point loading) (ASTM C78)*. USA: ASTM International.

[33] Jamshidi Avanaki, M., Abedi, M., Hoseini, A., & Maerefat, M. S. (2018). Effects of fiber volume fraction and aspect ratio on mechanical properties of hybrid steel fiber reinforced concrete. *Journal of New Approaches in Civil Engineering*, *2*(2), 49–64.

[34] Meza, A., & Siddique, S. (2019). Effect of aspect ratio and dosage on the flexural response of FRC with recycled fiber. *Construction and Building Materials*, *213*, 286–291. https://doi.org/10.1016/j.conbuildmat.2019.04.081

[35] Červenka, J., Červenka, V., & Laserna, S. (2018). On crack band model in finite element analysis of concrete fracture in engineering practice. *Engineering Fracture Mechanics*, *197*, 27–47. https://doi.org/10.1016/j.engfracmech.2018.04.010

[36] Das, A. (2023). *Analysis of pavement structures* (2nd ed.). USA: CRC Press.

[37] Ioannides, A. M. (2006). Concrete pavement analysis: The first eighty years. *International Journal of Pavement Engineering*, *7*(4), 233–249. https://doi.org/10.1080/10298430600798481

[38] Kausel, E. (2010). Early history of soil–structure interaction. *Soil Dynamics and Earthquake Engineering*, *30*(9), 822–832.

[39] Mahrenholtz, O. H. (2010). Beam on viscoelastic foundation: An extension of Winkler's model. *Archive of Applied Mechanics*, *80*(1), 93–102.

[40] Westergaard, H. M. (1926). Stresses in concrete pavements computed by theoretical analysis. *Public Roads, 7*(2), 25–35.
[41] Chen, M., Si, H., Fan, X., Xuan, Y., & Zhang, M. (2022). Dynamic compressive behaviour of recycled tyre steel fibre reinforced concrete. *Construction and Building Materials*, *316*, 125896. https://doi.org/10.1016/j.conbuildmat.2021.125896
[42] Younis, K. H. (2021). Metakaolin modified recycled aggregate concrete containing recycled steel fibers. *Materials Today Proceedings*, *45*, 4689–4694.
[43] Zhong, H., & Zhang, M. (2020). Experimental study on engineering properties of concrete reinforced with hybrid recycled tyre steel and polypropylene fibres. *Journal of Cleaner Production*, *259*, 120914. https://doi.org/10.1016/j.jclepro.2020.120914
[44] Yu, R., Spiesz, P., & Brouwers, H. J. H. (2014). Static properties and impact resistance of a green ultra-high performance hybrid fibre reinforced concrete (UHPHFRC): Experiments and modeling. *Construction and Building Materials*, *68*, 158–171. https://doi.org/10.1016/j.conbuildmat.2014.06.033
[45] Cladera, A., Weber, B., Leinenbach, C., Czaderski, C., Shahverdi, M., & Motavalli, M. (2014). Iron-based shape memory alloys for civil engineering structures: An overview. *Construction and Building Materials*, *63*, 281–293. https://doi.org/10.1016/j.conbuildmat.2014.04.032
[46] Shah, S. H. A., Ali, B., Ahmed, G. H., Tirmazi, S. M. T., El Ouni, M. H., & Hussain, I. (2022). Effect of recycled steel fibers on the mechanical strength and impact toughness of precast paving blocks. *Case Studies in Construction Materials*, *16*, e01025. https://doi.org/10.1016/j.cscm.2022.e01025
[47] Zhang, Y., & Gao, L. (2020). Influence of tire-recycled steel fibers on strength and flexural behavior of reinforced concrete. *Advances in Materials Science and Engineering*, *2020*(1), 6363105. https://doi.org/10.1155/2020/6363105
[48] Hu, H., Papastergiou, P., Angelakopoulos, H., Guadagnini, M., & Pilakoutas, K. (2018). Mechanical properties of SFRC using blended recycled tyre steel cords (RTSC) and recycled tyre steel fibres (RTSF). *Construction and Building Materials*, *187*, 553–564. https://doi.org/10.1016/j.conbuildmat.2018.07.206
[49] Gul, A., Alam, B., Iqbal, M. J., Ahmed, W., Shahzada, K., Javed, M. H., & Khan, E. A. (2021). Impact of length and percent dosage of recycled steel fibers on the mechanical properties of concrete. *Civil Engineering Journal*, *7*(10), 1650–1666. https://doi.org/10.28991/cej-2021-03091750
[50] Shokouhian, & Tsegaye. (2022). A parametric study on recycled steel fiber reinforced concrete. In *11th International Conference on Short and Medium Span Bridges*.
[51] He, W., Kong, X., Fu, Y., Zhou, C., & Zheng, Z. (2020). Experimental investigation on the mechanical properties and microstructure of hybrid fiber reinforced recycled aggregate concrete. *Construction and Building Materials*, *261*, 120488. https://doi.org/10.1016/j.conbuildmat.2020.120488

How to Cite: Ahmad, I., & Shokouhian, M. (2025). Promoting Sustainable Green Infrastructure: Experimental and Numerical Investigation of Concrete Reinforced with Recycled Steel Fibers. *Archives of Advanced Engineering Science*, *3*(4), 252–264. https://doi.org/10.47852/bonviewAAES42022837